Peripheral inflammation mediates midbrain Lrrk2 kinase activity via Rab32 expression

Jordan Follett*, Isaac Bul Deng*, Robert C. Sharp, Shannon Wall, Adamantios Mamais and Matthew J. Farrer

[1] Department of Neurology, McKnight Brain Institute, University of Florida, Gainesville, Florida, USA

To whom the correspondence should be addressed: Jordan Follett (Jordan.follett@neurology.ufl.edu) and Matthew J. Farrer (m.farrer@ufl.edu).

* Contributed equally to the study

Keywords: Evolution; LRRK2; RAB32, inflammation, Parkinson's Disease

Abstract =

Main text =

References =

Figures =

Supplementary figures =

Supplementary tables =

ABSTRACT

Parkinson disease (PD) is a neurodegenerative movement disorder that involves a complex interaction between genetic background, environmental exposures and ageing. Increased leucine-rich repeat kinase 2 (LRRK2) activity confers substantial risk for PD albeit with age-associated and incomplete penetrance that suggests other factors are required to manifest disease. We recently linked and associated RAB32 Ser71Arg as a Mendelian gene for PD. Here, we aimed to determine how Rab32 influences LRRK2 kinase activity and whether inflammatory stressors modulate this interaction in vivo. *In vitro* we show that the expression of Rab32 and Rab38 are modestly, but inversely, associated with their homologue Rab29. Both wild type RAB32 and to a greater extent, RAB32 Ser71Arg, promote the phosphorylation of Rab10, a *bonafide* LRRK2 kinase substrate. *In vivo*, we demonstrate murine *Rab32* expression increases in brain in response to inflammation induced by peripherally administered lipopolysaccharide (LPS). Further profiling of LPS-induced *Rab32* expression in micro-dissected brain tissue reveals regional specificity which is consistently elevated in the midbrain. In contrast, *Rab29* and *Rab38* expression are not immunoresponsive. Confocal microscopy analysis of midbrain dopaminergic neurons and Iba1^{+} microglia shows LPS-increased expression of Rab32 is largely restricted to Iba1^{+} microglia and localized to a Lamp1^{+} compartment. Most notably, LPS-induced *Rab32* expression in midbrain correlates with Lrrk2 kinase activity. Further, Rab32 expression is also induced by LPS in induced pluripotent stem cell-derived microglia from healthy control donors, demonstrating a unified biological response to inflammation across species. These data suggest that the penetrance of *LRRK2* PD is a function of peripheral inflammation, with important consequences for LRRK2 clinical trials aimed at neuroprotection. RAB32 is a physiologic and molecular rheostat of LRRK2 kinase activation.

INTRODUCTION

Leucine-rich repeat kinase 2 *(LRRK2)* mutations are a leading molecular cause of Parkinson's disease (PD) that is indistinguishable from the idiopathic condition. In North Africa, LRRK2.Gly2019Ser can be observed in 1/2,047 of the Arab-Berber population and in >30% of patients with PD.[1] Similarly, LRRK2 Arg1441Gly drives risk of PD in Basques[2], as does LRRK2 Gly2385Arg throughout Asia.[3] Each of these mutations largely originated from a single ancestral founder as their inheritance is identical-by-descent.[4,3,2] LRRK2 mutation frequencies in these specific populations have been driven by positive evolutionary selection, and represent an evolutionary adaptation of the human host to pathogen(s).[5] In mice, Lrrk2 mutations enhance peripheral immunity to provide a survival advantage to infection.[6,7] All pathogenic LRRK2 substitutions lower the threshold to stimulate its kinase activity but phosphorylate Rab GTPase substrates, which may dysregulate their localization and function.[8] Indeed, constitutive Lrrk2 kinase activity perturbs neurotransmission, endolysosomal trafficking and autophagy in neuronal synapses.[9] In humans, with age, LRRK2 kinase activating mutations may ultimately lead to the progressive loss of striatal dopaminergic (DA) terminals, axons and cell bodies in the *substantia nigra pars compacta* (*SNpc*) accompanied by gliosis and pleomorphic pathologies (alpha-synucleinopathy or tauopathy).[10,11] Hence, the successful development of Lrrk2 kinase inhibitors, now in clinical trials, may provide the first disease-modifying intervention.

However, the lifetime penetrance of mutant *LRRK2* is incomplete within families, variable and population-specific[12–14], and the physiologic factors responsible for LRRK2 kinase activity *in vivo* have yet to be fully defined. In transfected cells most LRRK2 remains inactive in the cytosol but its kinase is readily induced by RAB29 overexpression, by trafficking to membrane, dimerization and feed-forward amplification.[15,16] Group II RAB GTPases, including

RAB29 (formerly RAB7L1), RAB32 and RAB38 are highly homologous[17], and all three bind LRRK2 via its ankyrin domain for membrane recruitment.[18] Some polymorphic variants in *RAB29* modestly correlate with expression and are associated with PD[19,20] but endogenous Rab29 does not impact basal nor stimulated Lrrk2 kinase activity.[21] More recently, RAB32 Ser71Arg has been linked and associated with PD[22,23] and shown to increase LRRK2 kinase activity.[22] This mutation has been inherited, identical-by-descent, in worldwide families with multi-incident PD although its penetrance has yet to be defined. RAB32 Ser71Arg is most frequent in the Middle East, observed in 1/3,033 individuals, although this cause of PD has yet to be reported in these populations.[24]

Here we assess Rab29, Rab32 and Rab38 gene and protein expression in mouse brain, including the relationship between these homologues with Lrrk2 kinase activity, under basal conditions and with peripheral immune stimulation, and compliment this biology with induced pluripotent stem cell-derived microglia.

MATERIALS AND METHODS

Animals and housing

All animal procedures were performed in accordance with a protocol approved by the Institutional Animal Care and Use Committee (IACUC) at the University of Florida. Colonies were maintained on a reverse cycle (light on from 7pm to 7am) and single-sex group-housed in enrichment cages after weaning at post-natal day 21. All mice were supplied with rodent diet and water ad libitum. All experiments, data processing and analysis were conducted in a blinded manner. All lines are maintained on a C57BL/6J congenic background from Jackson Labs and have been back crossed >12 generations.

Cell lines, siRNA treatments, RNA and protein extraction

Mouse melanoma B16-F10 (CRL-6475; ATCC©) and human embryonic HEK293FT (R70007; Thermo Fisher Scientific©) cells were maintained at 37 °C/5 % CO2 in Dulbecco's Modified Eagles Medium (DMEM) from ATCC© (Cat #30-2002) and Thermo Fisher Scientific© (Cat #11965118), respectively, supplemented with 10% (v/v) FBS (Gibco©; 16140071) and 2mM Glutamax (Gibco©: 35050061). Cells were passaged every 2-3 days and passage number was maintained below 20 to limit cellular senescence.

For siRNA experiments, B16 cells were seeded in DMEM growth medium containing 25 nM pooled siRNA complexes in Nunc 6-well culture dishes (Thermo Fisher Scientific©; Cat # 140685) at 1 x10^6 per well. siRNA complexes against *Rab32 (*Catalog ID: L-063539-01-0020), *Rab38* (Catalog ID: L-040873-01-0020*), Rab29* (Catalog ID: L-053101-01-0020*)* and non-targeting control (Catalog ID:D-001810-10-20) were purchased from Dharmacon (Lafayette, CO, USA).

After seventy-two hours of transfection, cells were processed for RNA extraction using a RNeasy® Mini Kit (Qiagen©) or protein extraction using ice-cold 1x Cell Signaling Lysis Buffer (Cell Signaling Technology© #9803S) supplemented with Halt phosphatase inhibitor cocktail (Thermo Fisher Scientific©), and protease inhibitor cocktail (Roche©) and left on ice for 30 min to lyse. Lysates were clarified at 20,000 g for 10 min at 4 °C and pelleted debris were removed. Samples were supplemented with NuPage LDS sample buffer 4x (NP0008), boiled for 5 min at 95 °C and analyzed by standard western blot protocols.

cDNA, Transfection, co-immunoprecipitation and Western blot (WB)

The following plasmids were used for cell transfection assays and were generated by the MRC PPU Reagents and Services at the University of Dundee (https://mrcppureagents.dundee.ac.uk). Each construct was confirmed by sequencing at the MRC Sequencing and Services (https://www.dnaseq.co.uk). All plasmids are available to request via the MRC PPU Reagents and Services website (https://mrcppureagents.dundee.ac.uk). HA-RAB32 Ser71 wild-type (DU52622); HA-RAB32 Arg71 (DU77801); HA-RAB32 Q85L (DU77209) and HA-RAB32 T39N (DU76462); HA-empty vector (Addgene Plasmid #128034).

For LRRK2 activation assays, HEK293FT cells seeded into 6-well dishes were transiently co-transfected at 70–80% confluence with 3xFLAG-tagged LRRK2 wild type, HA-empty, HA-RAB32 or variant plasmids using Lipofectamine 2000 transfection reagent (Thermo Fisher Scientific©). Forty-eight hours after transfection, medium was replaced in all experimental wells where a subset of neighboring wells received 200nM MLi-2 (Tocris Bioscience©; 5756 dissolved in DMSO) prior to lysis in Cell Signaling Lysis Buffer (Cell Signaling Technology© #9803S) supplemented with Halt phosphatase inhibitor cocktail (Thermo Fisher Scientific©), and protease inhibitor cocktail (Roche©) and left on ice for 30 min to lyse. Lysates were clarified at 20,000 g for 10 min at 4 °C and pelleted debris were removed. Samples were supplemented with NuPage LDS sample buffer 4x (NP0008), boiled for 5 min at 95 °C and analyzed by standard western blot protocols.

For co-immunoprecipitation experiments, cells seeded in 10cm culture fishes were transfected with 10ug of HA-empty, HA-RAB32 or variant plasmids using Lipofectamine 2000 transfection reagent (Thermo Fisher Scientific©) and lysed 24 hr post-transfection in ice-cold lysis buffer containing 50 mM Tris-HCl pH 7.4, 150 mM NaCl, 1 mM EGTA, 270 mM sucrose and 0.1% (v/v) NP40-alternative, supplemented with Halt phosphatase inhibitor cocktail (Thermo Fisher Scientific©), and protease inhibitor cocktail (Roche) and left on ice for 30 min to lyse. Clarified lysate was used to immunoprecipitate HA-Rab proteins with 25 µL Pierce™ Anti-HA Agarose resin (Thermo Fisher Scientific©; Cat # 26181) for 1 hr at 4°C. Immunoprecipitates were washed three times with lysis buffer and eluted in 2x NuPage LDS sample buffer (NP0008), boiled for 5 min at 95 °C and analyzed by standard western blot protocols.

Peripheral injection of lipopolysaccharide (LPS) in C57BL/6J mice

LPS was purchased from Cell Signaling Technology (14011), and reconstituted in sterile PBS to a working stock of 1mg/ml. To obtain volumes suitable for intraperitoneal injection (i.p.) of LPS, the stock solution was diluted in sterile PBS to a concentration of 0.5mg/ml or 0.1mg/ml, filtered with Millex filter unit (0.22 um) and injected in sterile glass vials to be used during injection to limit contamination. Mice were injected with a single dose of 5mg/kg of LPS, or 2 subsequent doses of 1mg/kg LPS (24 hr apart), then euthanized for tissue collection via inhalation of isoflurane at 6 and 24 hr after the last dose. Control mice were given saline.

Brain extraction and homogenization for RNA and protein extraction

Mice were euthanized by isoflurane inhalation and transcardially perfused with ice-cold phosphate-buffered saline (PBS). Harvested brains were generally midline dissected with one

hemisphere drop-fixed in 4% paraformaldehyde (PFA) in PBS for 24 hr for subsequent immunofluorescence (IF) while cortex (CTX) and midbrain (MB) were micro-dissected from the other hemisphere, and snap-frozen in liquid nitrogen for quantitative polymerase chain reaction (qPCR) and/or western blotting. For a separate cohort, brains were cut at the midbrain into left and right hemispheres, and micro-dissected into prefrontal cortex (PFC), striatum (STR), hippocampus (HP), midbrain (MB), lower brainstem (BS; both pons and medulla) and cerebellum (CB) to examine regional gene expression of immunoregulation and Rab GTPase genes. Snap-frozen brain sections designated for RNA extraction were first mechanically homogenized in RLT buffer (provided in the RNeasy® Mini Kit [Qiagen©]) with a glass mortar and was further homogenized using QIAshredder (Qiagen©) tubes. After homogenization, brain tissues underwent RNA extraction/isolation following the protocols provided by the RNeasy® Mini Kit, where homogenates were treated with 70% ethanol and RNA was captured and washed within the mini spin columns provided. Pure RNA was eluted into separate 1.5 microcentrifuge tubes from the mini columns with 50 μL of RNase-free water (provided by the RNeasy® Mini Kit) and each sample was then quantified (ng/uL) using a NanoDrop™ One/One^{C} spectrophotometer (Thermo Fisher Scientific©). All RNA samples were kept in aliquots frozen in a -80 °C freezer until ready for use. Brain tissues designated for protein extractions were homogenized in RIPA Lysis Buffer (Pierce® # 89900) supplemented with Halt™ Protease and Phosphatase Inhibitor Cocktail (100x; Thermo-Fisher™: 78440) in a 1 ml glass Dounce homogenizer (Wheaton) and allowed to rotate at 4°C for 45 min on HulaMixer before centrifugation (14,000 × *g* at 4 °C for 15 min). Supernatant was aliquoted appropriately to help mitigate freeze-thawing cycles. Homogenate aliquots and the resulting pellets were frozen separately and stored in a -80 °C freezer.

Single strand complementary DNA (cDNA) synthesis and quantitative PCR

RNA samples from cohorts of mice and B16 cell lines were converted into cDNA by use of the High-Capacity cDNA Reverse Transcription Kit (Applied Biosystems™). Briefly, in a 384-well plate, a mixture containing 10 μL of total cDNA master mix (10X RT Buffer, 10X RT Random Primers, 25x dNTP Mix [100 mM], MultiScribe™ Reverse Transcriptase [50 U/μL]) and 10 μL of 400 ng of RNA (diluted with RNase-free water) were dispensed across three wells per mouse/cell line per gene examined (3 technical replicates). The 384-well plate was then sealed with optical tape and placed in a VeritiPro™ 384-well Thermal Cycler (Applied Biosystems™) to undergo reverse transcription using recommended conditions in the High-Capacity cDNA Reverse Transcription Kit manual. After cDNA conversion, 4 μL from each well were pipetted into a new 384-well plate, where 10 μL of TaqMan™ Universal Master Mix II, with UNG (Applied Biosystems™), 5 μL of RNase/DNase-free water, and 1 μL of TaqMan™ Gene Expression Assay (Thermo Fisher Scientific©) was added in three wells per mouse/B16 cell line, per gene examined. TaqMan™ Gene Expression Assays used were: glyceraldehyde-3-phosophate dehydrogenase (*Gapdh*): Mm99999915_g1; beta-actin (*Actb*): Mm02619580_g1; *Ionized calcium binding adaptor molecule 1* (*Aif1/Iba1*): Mm00479862_g1; glial fibrillary acidic protein (*Gfap)*: Mm01253033_m1; immune-response gene 1 (*Irg1*): Mm01224532_m1; Lysosome-associated membrane protein 1 (*Lamp1*): Mm01217070_m1; Signal transducer and activator of transcription 1 (*Stat1*): Mm01257286_m1; *Lrrk2*: Mm00481934_m1; *Rab20*: Mm01216807_m1; *Rab29*: Mm00523103_m1; *Rab32*: Mm00458960_m1; *Rab38*: Mm00503697_m1. Once cDNA and TaqMan™ master mixes were pipetted, the 384-well plates were placed into a QuantStudio™ 5 Real-Time PCR System (Applied Biosystems™), where QuantStudio™ Design & Analysis Software (Applied Biosystems™) was used to conduct qPCR

and find comparative Ct values (ΔΔCt) from each well using the standard protocols supplied in the software. For each mouse/B16 cell line examined on the qPCR plates, the combined mean of Ct values from the housekeeping genes *Gapdh* and *Actb* were calculated and ΔCt was found for each targeted gene from each sample (ΔCt = Ct value of targeted gene – Ct value of combined mean *Gapdh* and *Actb*). To compare groups from saline controls (mice cohorts) and no template controls [NTC] (B16 cell line), the ΔΔCt method was used, where ΔΔCt = ΔCt of targeted gene from experimental group – ΔCt of targeted gene from control group. Once ΔΔCt was found for each comparison, relative gene expression for the gene of interested in each sample was calculated using $2^{(-\Delta\Delta Ct)}$.

Western blotting

Protein samples were subjected to Pierce™ BCA Protein Assay Kit (Thermo Scientific™), protein concentration were then calculated and samples reduced with NuPage™ LDS Sample Buffer 4x (#NP0008) for 5 min at 95 °C. Samples were then analyzed by standard Western blotting, as previously described[25], using primary antibodies detailed in **Supplemental Table 1**. Secondary antibodies were used at 1:10,000 dilution: IRDyes® 800CW Goat anti-Rabbit IgG (Li-Cor Biotech©; #926–32211) and 680RD Goat anti-Mouse IgG (Li-Cor Biotech©; #926–68070). Raw blots were quantified using ImageJ's western blotting algorithm to determine the stained area under the curve and normalized to the levels of Gapdh.

Immunofluorescence with confocal microscopy

Brains (24 hrs time point only) were fixed in 4% paraformaldehyde (PFA) overnight at 4°C, and cryoprotected with 30% sucrose in PBS before 30 µm sagittal slices were obtained with a

cryostat. Sections were blocked in 10% normal goat serum (NGS) in 0.3% PBS-triton-X 100 (PBST) (1h, 37°C), followed by overnight (4°C) incubation of primary antibodies, described in **Supplemental Table 1,** diluted in 5% NGS + 0.3% PBST. The sections were washed (4×15 min in PBS), followed by secondary antibody incubation with species-specific Alexa Fluor™ IgG secondary antibodies for 1h at RT (Invitrogen©, 1:500). Tissues were rewashed in PBS (4 × 15 min), then co-stained with DAPI (Thermo Fisher Scientific©,1:5000) and mounted using Fluoromount-G™ (00-4958-02, Invitrogen©). Images were acquired at 60x field of view on a Nikon® Spinning Disc Confocal Microscope (AX/AX R with NSPARC) using NIS-Elements AR Imaging software from Nikon® (90 z-stack steps at 0.30 μm spacing), with its intrinsic deconvolution function Th, Iba1, Lamp1 and Rab32 immunoreactivity in the MB was quantified with the Imaris™ software (Oxford Instruments). Briefly, Th^+ DA neurons (smoothing: 0.3 μm) and $Iba1^+$ microglia (smoothing; 0.10 μm) were rendered as surfaces, and the AI component of the Imaris™ software was used for unbiased identification of Th^+ DA neurons and $Iba1^+$ microglia - only whole cells in the field of view were included in the analysis as identified with DAPI. The microglia projections that broke off from their somas were stitched, and the volume of Th^+ DA neurons and $Iba1^+$ microglia were quantified accordingly. Similarly, Lamp1 (smoothing: 0.100 μm, threshold value: 500 and number of voxels: 10) and Rab32 puncta (smoothing: 0.100 um, threshold value: 250, and number of voxels: 10) were rendered as surfaces, their volumes were quantified accordingly and normalized to the total volumes of Th and/or Iba1.

Differentiation of human iPSCs into microglia

Human iPSCs were maintained feeder-free in StemFlex medium (Thermo Fisher) on Matrigel-coated plates and passaged with Accutase. The microglia differentiation protocol was adapted

from[26]. Briefly, 10,000 cells/well were seeded into 96-well ultra-low attachment plates in embryoid body (EB) medium (E8 supplemented with 10 µM ROCK inhibitor, 50 ng/ml BMP-4, 20 ng/ml SCF, 50 ng/ml VEGF-121) and centrifuged (300 g, 3 min). EBs were cultured for 4 days with a half-medium change on day 2. On day 4, EBs were transferred to 6-well plates (20/well) in microglia progenitor medium consisting of X-VIVO 15 media (Lonza; 02-053Q) supplemented with 2 mM GlutaMax, 55 µM β-mercaptoethanol, 100 ng/ml M-CSF, 25 ng/ml IL-3). Medium was refreshed twice weekly. Progenitors appeared between days 7–21 and were harvested from suspension. Progenitors were plated in microglia maturation medium consisting of Advanced RPMI 1640 (Thermo Fisher Scientific) with 2 mM GlutaMax, 100 ng/ml IL-34 (PeproTech), and 10 ng/ml GM-CSF (PeproTech). Cells adhered within 1–2 h and matured into microglia over 6–10 days. Parent EB cultures continued to produce progenitors for up to 3 months with regular feeding. All cytokines were from PeproTech unless otherwise specified. For LPS treatment experiments, progenitors were plated at 150,000 cells per well in a 24-well plate, and following 6-10 day culture in maturation media microglia cells were treated with 100 ng/mL LPS for 24 hrs prior to fixation and ICC.

Nomenclature and statistical analysis

By convention all human gene names are italicized and capitalized, whereas mouse gene names only have the first letter capitalized, whereas the protein's encoded are written as standard text. Experiments examining relative gene expression between B16 cells following siRNA-mediated knockdown were analyzed using a repeated-measures one-way ANOVA with a Tukeys multiple comparisons post hoc test. Experiments examining relative gene expression between mice cohorts were analyzed using either a Brown-Forsythe and Welch ANOVA tests with a Dunnett's T3 multiple comparisons post hoc test (parametric data), a Kruskal-Wallis test with a Dunn's

multiple comparisons post hoc test (nonparametric data), or a two-way ANOVA with a Tukey multiple comparisons post-hoc test, where figure legends indicate which was specifically used for that experimental group. Experiments examining phosphorylation and total protein levels by immunoblotting were analyzed by one- or two-way ANOVA with Tukey's *post-hoc* test. Immunohistochemical images were analyses via unpaired *t*-test. All statistical analyses were performed using GraphPad Prism for Windows (GraphPad Software, San Diego, CA). Mean values ± S.E.M are presented with each dot on the graph representing an individual experimental unit.

RESULTS

Validation of commercially available Rab antibodies

We initially evaluated commercially available antibodies raised against Rab32, Rab38 and Rab29 in a murine cell line, given the close sequence homology of Group II sub-family of GTPases.[17] B16 cells plated in siRNA-containing medium against *Rab32*, *Rab38*, *Rab29* or a non-targeting control (NTC) for 72 hours were processed for analysis by WB. While the siRNA-mediated loss of Rab32, Rab38 or Rab29 protein confirmed the specificity of commercially available antibodies, there was a modest but significant, inverse relationship between the levels of Rab29 and those of Rab32 and Rab38 **(Figure 1)**. Knockdown of Rab32 protein levels to <0.01 of that observed in NTC cells did not significantly alter Rab29 or Rab38 (compare **Figure Bi-iii**). In contrast knockdown of Rab38 protein to <0.10 of that observed in NTC cells was accompanied by a 0.3-fold (± S.E.M 0.10) decrease in Rab32 although Rab29 levels remained unchanged (compare **Figure 1Biii** with **Bi** and **Bii**). Knockdown of Rab29 protein to <0.05 of that observed in NTC cells also lead to significant 1.6-fold (± S.E.M 0.07) increase in Rab32 and 1.25-fold (±

S.E.M 0.06) increase in Rab38 (compare **Figure 1Bii** with **Bi** and **Biii**). There was no significant difference in level of total Lrrk2 with any of these siRNA treatments (**Figure 1Biv & C**). The phosphorylation of Rab10 at a known Lrrk2 phosphorylation site (pThr73-Rab10) remained comparable to NTC levels with the knockdown of Rab32 and Rab38 but was significantly increased 2-fold (± S.E.M 0.13) with the knockdown of Rab29 (**Figure 1Bv**). While this may seem contrary to the literature [21], the activation of Lrrk2 kinase observed is consistent with the modest, reciprocal elevation in Rab32 and Rab38 when Rab29 is knocked down (**Figure 1Bi and 1Biii**). Lamp1 levels were slightly but significantly diminished 0.18-fold (± S.E.M 0.06) compared to NTC cells with Rab32 knockdown, whereas Lamp1 levels significantly increased 1.25 (± S.E.M 0.11) and 1.34-fold (± SEM 0.13) with Rab38 and Rab29 knockdown, respectively (**Figure 1Bvi**).

Complementary observations were made by qPCR that confirmed siRNA-mediated loss of Rab32, Rab38 and Rab29, albeit with no significant impact on the expression of *Lrrk2* (**Figure 1C**). In addition, modest differences in gene expression were observed across the individual Rabs that reflect observations made for their respective proteins; *Rab29* knockdown leads to a significant increase in *Rab32* and *Rab38* gene expression (RM-ANOVA, $F_{1.400, 15.40} = 47.94$, $p < 0.05$ and $F_{2.122, 23.35} = 53.69$, $p < 0.01$, respectively) suggesting their expression is controlled by transcription (compare **Figure 1Ci** and **Cii**). The knockdown of *Rab38* modestly decreased the expression of *Rab32* and *Rab29* **(Figure Ci** and **Ciii**), while the knockdown of *Rab32* decreased *Rab38* but not *Rab29* expression (**Figure Cii** and **Ciii**). Lastly, the knockdown of *Rab32* but not *Rab38* significantly decreased the expression of *Lamp1*, while the knockdown of *Rab29* had the opposite effect on *Lamp1* expression (**Figure Cv**).

HRP-conjugated mouse monoclonal antibodies raised against Rab32 and Rab38 gave similar increases in the expression Rab32 and Rab38 with knockdown of Rab29 **(Supplementary Figure 1A).** Thus, as a complimentary approach, B16 cells grown on coverslips for knockdown of Rab32, Rab38, Rab29 or a non-targeting control (NTC) were processed for immunocytochemistry (ICC) and confocal microscopy **(Supplementary Figure 1B &C)**. The sub-cellular distribution of Rab29, Rab32 and Rab38 is quite distinct although close homologues. Consistent with published literature[19], most endogenous Rab29 was perinuclear, reminiscent of the Golgi apparatus, and signal intensity diminished with Rab29 siRNA. Confocal microscopy of endogenous Rab38 displayed a more diffuse albeit discrete, punctate endosomal staining, that also responded to siRNA-mediated knockdown. In contrast, endogenous Rab32 displayed an exclusive, perinuclear punctate staining that was subsequently confirmed to be Lamp1^{+} compartment, potentially lysosomes **(Supplementary Figure 1B, C & D)**. Together, these data validate the commercially available antibodies raised against murine Rab29, Rab32 and Rab38 used throughout this study, and uncover a novel relationship between the levels of Rab29, Rab32 and Rab38 and their ability to promote Rab10 phosphorylation.

Rab32 is upstream of Rab38 and Rab29 and is necessary to support Lamp1 and Rab10 phosphorylation

To better understand the functional relationship between Rab29, Rab32, Rab38 and their influence on pT73-Rab10 and Lamp1, B16 cells were plated in siRNA-containing medium against *Rab32*, *Rab38*, *Rab29* or a non-targeting control (NTC) or equimolar concentrations of *Rab38* and *Rab29*, *Rab32* and *Rab29* or *Rab32* and *Rab38* for 72 hours before being processed for analysis by WB (**Supplementary Figure 2**). Consistent with individual targeting siRNA

experiments, the co-knockdown of Rab38 and Rab29 or Rab32 and Rab38 did not significantly alter the level of Rab32 (**Supplementary Figure 2 Bi**) or Rab29 (**Supplementary Figure 2 Bii)**, respectively. The levels of Rab38 were significantly increased following the knockdown of Rab29, however this increase in Rab38 reverted to non-targeting control levels upon co-knockdown of Rab29 and Rab32 (**Supplementary Figure 2 Biii)**. There were no significant differences in level of total Lrrk2 with any of these siRNA treatments (**Supplementary Figure 2 Biv**). In contrast, while the knockdown of Rab29 lead to a significant increase in pT73-Rab10/Rab10 levels, this increase was diminished upon co-knockdown of Rab38 and Rab29, Rab32 and Rab29, and Rab38 and Rab32 (**Supplementary Figure 2 Bv**). Lamp1 levels were significantly increased following the co-knockdown of Rab38 and Rab29; the co-knockdown of Rab32 and Rab29 normalized the increased levels of Lamp1 observed following the knockdown of Rab29 alone while the co-knockdown of Rab32 with Rab38 significantly reduced the levels of Lamp1 (**Supplementary Figure 2 Bvi)**. Together, these results suggest that Rab32 is likely upstream of Rab38 and necessary to promote Rab10 phosphorylation and Lamp1 biogenesis.

Peripheral administration of LPS increases Rab32 expression and Lrrk2 kinase activity

Recent studies have suggested *LRRK2* and *RAB32* expression are immunoresponsive, and that RAB32 promotes LRRK2 kinase activity.[27,22] To establish a robust model of inflammation, three-month-old male C57BL/6J WT mice were injected with a single dose of LPS at 5mg/kg, or two single doses of 1mg/kg 24 hr apart, with saline as a control (**Supplementary Figure 3**). Brains were harvested at 6 or 24 hr after the last injection. When assessed by qPCR, all mice that received LPS had a significant increase in the levels of *Irg1*, a known immune-responsive

gene/protein that is upregulated during inflammation to produce an anti-microbial metabolite (**Supplementary Figure 3B**). However, only mice that received two doses of 1mg/kg LPS had a robust increase in the expression of *Iba1* and *Gfap*, two well documented markers of gliosis. To compliment these results, tissue from LPS-injected mice were homogenized and analyzed by WB. Relative to mice that received saline control, and using 2x 1mg/kg LPS, the levels of Iba1 and Stat1 were significantly increased by 24 hours but not at the 6 hour time point. Mice that received a single dose of LPS at 5mg/kg responded similarly, as indicated by their behavior and weight loss (**Supplementary Figure 3A**). However, their levels of Iba1 and Stat1 within the CNS were unaltered (**Supplementary Figure 3B-D)**. These findings suggest immune priming using two successive LPS applications is necessary to induce robust CNS inflammation. As a control we analyzed neuronal markers, namely tau and α-synuclein, which remained unaltered by exposure to LPS. Overall, these results suggest that delivery of 2x 1mg/kg of LPS via intraperitoneal injection is sufficient to drive acute inflammation within the CNS without compromising neuronal integrity (**Supplementary Figure 3A-D)**.

Having established a working inflammation paradigm, we asked whether peripheral inflammation contributes to the expression of Rab32 and Lrrk2 kinase activity *in vivo* within the CNS. Three-month-old male C57BL/6J WT mice were injected with two single doses of LPS at 1mg/kg or saline control 24 hr apart, and their brains were harvested at 6 or 24 hr after the second injection. Initially, we focused on the midbrain of LPS and saline injected mice as gliosis and nigral neuronal loss are pathologic hallmarks of PD. To ensure that our peripheral inflammatory paradigm was sufficient to induce CNS inflammation, and to validate previously published observations[27], we performed qPCR on the midbrain of WT mice that received LPS

(2x 1mg/kg at baseline 0, 6 and 24 hr). As expected, the relative gene expression for *Irg1* rapidly increased within 6 hours following LPS exposure, and throughout the brain, but reverted to near saline levels within 24 hours of LPS exposure (**Figure 2A and Supplementary Figure 4**). Similar to *Irg1,* expression of the transcription factor *Stat1* rapidly increased within 6hrs of LPS exposure but reverted to near saline levels by 24 hours (**Figure 2A).** *Iba1* and *Gfap*, two well documented markers of gliosis, also increased following peripheral injection with LPS. Within other sections of the brain, upregulation of *Gfap* was significant in the prefrontal cortex and striatum but not in the lower brainstem, whereas *Iba1* was especially elevated in the striatum, midbrain and lower brainstem (**Figure 2A and Supplementary Figure 4**). Gfap and Iba1 protein levels in the midbrain were significantly elevated by 24 hrs (**Figure 2C**). We next assessed the expression profiles of *Rab20* (a published positive control[27]), *Rab32, Rab38, Rab29* and *Lrrk2* in the midbrain of saline and LPS injected mice. The relative gene expression of *Rab20* modestly increased at 6 hours following LPS exposure, with the greatest change in the midbrain and striatum. *Rab20* gene expression reverted to the level of saline control within 24 hrs (**Supplementary Figure 4**) although the protein remained elevated (**Figure 2C**). The relative gene expression of *Rab32* significantly increased throughout the brain within 6 hours of LPS exposure and remained elevated in prefrontal cortex and hippocampus at 24 hrs (**Supplementary Figure 4**), and in midbrain the corresponding levels of protein were significantly elevated (**Figure 2C)**. In contrast, *Rab29 and Rab38* gene levels were not significantly increased by LPS-treatment in any brain region **(Supplementary Figure 4**); midbrain Rab29 protein levels were comparable to the saline control, although Rab38 protein levels appeared marginally, albeit non-significantly, elevated (**Figure 2C**). *Lrrk2* gene expression following LPS exposure remained unchanged at 6 and 24 hours, and protein levels were also unchanged (**Figure 2C,**

Supplementary Figure 4). Together, these results demonstrate peripheral administration of LPS is sufficient to drive the selective and sustained expression of *Rab32* in midbrain of WT mice. The $\log_2$ fold change (FC) of relative gene expression ($2^{(-\Delta\Delta Ct)}$) post-LPS for each gene has been mapped to a sagittal ideogram of the mouse brain (**Figure 3**, ideogram courtesy of the GENESTAT Project, and **Supplementary Figure 5**). Comparative statistical analysis of gene expression with/without peripheral LPS treatment (6hr and 24hr), within all 6 brain regions, is also provided by two-way ANOVA (**Supplemental Table 2)**.

Next, we assessed the levels of phosphorylated Rab10 (Thr73) normalized to total Rab10 protein, which is an accepted marker of Lrrk2 kinase activity.[28] Phosphorylated Thr73 Rab10 was significantly increased 24 hrs after 2x 1mg/kg LPS injections, relative to saline control (**Figure 2C**). Phosphorylated Thr73 Rab10 levels were highly correlated with Rab32 levels ($F_{1,24}$=20.85, r^2=0.47, $p<0.0001$, n=26), similar to the correlation for midbrain protein expression of Iba1 ($F_{1,24}$=19.14, r^2=0.44, $p<0.0002$, n=26). Hence, peripheral administration of LPS upregulates inflammatory markers within the CNS of WT mice, including GTPase Rab32 that promotes Lrrk2 kinase activity.

Membrane localization is necessary to promote Rab32 stability and activate LRRK2 kinase

To evaluate the role of Rab32 in LRRK2 kinase activation, we employed a HEK293 cell system previously used to assess LRRK2 kinase activity on Rab GTPases substrates.[29] We determined whether LPS-induced RAB32 expression is sufficient to drive LRRK2 kinase activation or if the complex requires membrane targeting. Hemagglutinin (HA)-RAB32 wild type, the GTP-locked Gln85Leu, GDP-locked Thr39Asn or pathogenic Ser71Arg variants were co-overexpressed with

wild type LRRK2 to assess the impact on LRRK2 kinase conformation (pSer935), autophosphorylation (pSer1292) and substrate phosphorylation (Rab10-Thr73). As a control, neighboring wells of transfected cells were treated ± MLi-2, a specific LRRK2 Type-I inhibitor, to demonstrate that the observed phosphorylation of Rab10 was directly mediated by LRRK2. As previous[29], overexpression of wild type RAB32 increased LRRK2-mediated Rab10 phosphorylation ~3-fold without enhancing pSer1292 autophosphorylation or inducing the dephosphorylation of pSer935 when compared to over-expression of LRRK2 alone (**Figure 4A & B**). Over-expression of the RAB32 Gln85Leu mutant produced a similar increase in Rab10 phosphorylation without changes in Ser1292 autophosphorylation or pS935 dephosphorylation while the GDP-locked RAB32 Thr39Asn mutant failed to induce changes in all three biochemical readouts of LRRK2 activity and is less stable than its WT counterpart (**Figure 4C)**. As a positive control, over-expression of RAB32 Ser71Arg increased the phosphorylation of Rab10 by ~6-fold with a concomitant ~2-fold increase in pSer1292 autophosphorylation and a modest dephosphorylation of the pSer935 (**Figure 4B**). In light these results, we performed co-immunoprecipitation on lysates from HEK293 cells transiently expressing HA-RAB32 WT, Gln85Leu, Thr39Asn or Ser71Arg, and resolved the immunoprecipitated complexes by WB. When compared to HA-RAB32 WT, the Gln85Leu and Ser71Arg variants co-immunoprecipitated endogenous LRRK2 to modestly higher levels, while the Thr39Asn variant reduced the interaction between RAB32 and LRRK2. Taken together, these results suggest that membrane targeting rather than the increased expression of RAB32 alone is necessary to promote LRRK2 activity.

Peripheral administration of LPS increases Rab32 expression in microglia

Basal Rab32 expression is highest in immune cells, including microglia, according to publicly available datasets[30] (Human Protein Atlas proteinatlas.org). However, our data suggests the RAB32-LRRK2 complex requires membrane association. Thus, we quantified the levels of Rab32 and Lamp1 in Iba1$^+$ microglia and Th$^+$ DA neurons in sagittal brain sections from WT mice injected with LPS using immunohistochemical methods. Peripheral administration of LPS induced microgliosis, as indicated by the retraction of microglia processes and enlarged cell bodies (**Figure 5A**), and elevated total Rab32 immunoreactivity in the midbrain (**Figure 5B**), complementary to the biochemical results. In addition, the total Lamp1 immunoreactivity was comparable between saline and LPS-injected mice (**Figure 5B**). Interestingly, microglial Lamp1 and Rab32 were all elevated with LPS, as well as the levels of Rab32 on Lamp1$^+$ puncta (**Figure 5B**). This was not the case for Th$^+$ DA neurons as the levels of Lamp1 and Rab32 were unaltered with LPS (**Figure 5C, D**).

Rab32 expression is increased in iPSC-derived microglia following exposure to LPS

Data from our murine model indicates that peripheral administration of LPS induces an upregulation of Rab32 expression in microglia within the midbrain (**Figure 5**)**.** To validate these findings and extend our observations to a human-relevant cellular model, we generated iPSC-derived microglia from healthy donors. Following treatment with LPS (100ng/mL; 24hrs) or saline control, iPSC-derived microglia were fixed and stained with antibodies against Rab32 and Iba1. Iba1immunoreativity was observed in > 95.0% of cells across both treatment conditions and exposure to LPS induced a more polarized microglia phenotype. Relative to saline control, LPS treatment significantly increased total Rab32 immunoreactivity in iPSC-derived microglia

(**Supplementary Figure 6**). These results suggest that LPS is sufficient to induce Rab32 expression in iPSC-derived microglia and provides a disease-relevant platform for therapeutic interventions.

DISCUSSION

Recent studies suggest RAB29 is the main GTPase responsible for LRRK2 recruitment to membrane for kinase activation[19,15,29]. In part, this originated from a modest genetic association between common variants in the *RAB29* locus and PD[19], which remains robust (rs11557080 A>G odds ratio (OR) = 1.12, 95% CI 1.09-1.16, p=1.85E-11).[31] Nevertheless, Lrrk2 kinase activity is not attenuated in Rab29 germline knock out mice.[21] Furthermore, genetic data now links its homologue, RAB32 Ser71Arg as a Mendelian gene for PD and, by association, this mutation has a much greater effect on the likelihood of PD (OR = 13.17, 95% CI 2·15–87·23, p=0.0055) leading to a 2-fold increase in LRRK2 kinase activity.[22] Rare variants in RAB29 and RAB38 that activate LRRK2 kinase have yet to be linked or associated with PD. Here we demonstrate RAB32 specifically localizes to a Lamp1+ve compartment, in contrast to RAB29 and RAB38, consistent with the major role of LRRK2 in endolysosomal autophagy.[32] Notably, our *in vitro* results suggest that transiently lowering Rab29 leads to a modest compensatory increase in Rab32 or Rab38 protein expression, but not vice versa, with analogous findings by gene expression. Silencing Rab29 also leads to a significant increase of pThr-Rab10/Rab10 arguing against its requirement for physiological Lrrk2 membrane recruitment and kinase activation. The amount of Lamp1 protein also significantly increases when Rab29 or Rab38 are silenced but marginally diminishes when Rab32 is silenced, suggesting a dependency on the latter and,

intriguingly, the transcription levels of Lamp1 appears to mediate this effect. Hence, Rab32 is the only Group II GTPase with immune-responsive expression.

In vivo peripheral LPS results in almost immediate transcriptional upregulation of inflammatory markers in the brain, including *Iba1*, *Gfap*, *Rab20* and *Rab32* within 6 hrs of last administration, of which *Iba1* and *Rab32* levels remained elevated at 24 hrs in close agreement with prior results.[27] Corresponding midbrain protein levels appeared to be highly correlated albeit temporally delayed, with Iba1, Stat1, Rab20 and Rab32, all significantly elevated 24 hrs post LPS exposure. Although Lrrk2 protein levels did not change with this stimulus or over this time course, Lrrk2 kinase activity (measured as the ratio of pThr73-Rab10/Rab10) was also highly correlated with the elevation of Rab32 (r^2=0.46, $p<0.0001$). Additional regional analysis of gene expression demonstrated Rab32 was upregulated in the lower brainstem, midbrain, hippocampus and prefrontal cortex within 6 hrs, and maintained its elevated expression at 24 hrs. How closely this effect may be associated with LPS dosing, and how long it lasts after administration requires further study.

In vitro cell culture and immunoprecipitation studies demonstrate Lrrk2 kinase activity requires membrane recruitment. All three homologues, RAB29, 32 and 38, specifically bind LRRK2 through its ankyrin domain, and are capable of recruiting LRRK2 monomer to membrane. Nevertheless, each of these RAB GTPases localizes to different intracellular compartments namely the Golgi, endoplasmic reticulum or Lamp1+ve vesicles, potentially lysosomes, respectively. Whether one specific membrane interaction is more relevant for the pathogenesis of PD remains unclear. *In vivo*, in the adult mouse brain and under non-inflammatory conditions,

Iba+ve microglia typically have a small cell body with highly ramified branches. Here peripheral LPS treatment appears to induce a hyper-ramified state associated with Rab32 and Lamp1 upregulation. Complimentary results, most notably an increased expression of Rab32 following acute treatment with LPS, were observed in iPSC-derived microglia from healthy donors (**Supplementary Figure 6**). In midbrain microglia there was also a highly significant co-localization of these markers on Lamp1+ vesicles, potentially lysosomes, that was concomitantly associated with increased Lrrk2 kinase activity. In contrast, neither the Rab32 nor Lamp1 within dopaminergic neurons was significantly increased with LPS treatment. Activated microglia are known to mediate non-cell-autonomous inhibition of neuronal autophagy via paracrine signaling[33], but how Rab32 levels influences cytokine secretion in the peripheral immune system[34,35] and microglia has yet to be established.

Subsequent review of murine and human Rab32 genomic sequences revealed tandem 5' transcription factor 3 (TFE3) E-box sequences (CANNTG)[36] within ~110 bp of the transcription start site (TSS) (**Supplementary Figure 7**). Rab29 and Rab38 have less conserved 'coordinated lysosomal expression and regulation' consensus motifs (CLEAR, namely GTCACGTGAC)[37] and none in tandem nor proximal to their TSS. Similarly, only RAB32 has tandem E-box and CLEAR sequences ~110bp proximal to its TSS, consistent with optimal TFEB/TFE3 transcription factor recognition.[38] Both transcription factors are associated with lysosomes in a phosphorylated state, in part, mediated by RAB32, mTOR activity and nutrient sensing to downregulate autophagy.[39,40] However, infection in myeloid-cells increases TFEB and TFE3 binding to CLEAR motifs located in the promoters of many lysosomal and proinflammatory genes to increase their expression.[41,42] LRRK2 kinase activity has been shown to modulate the

expression and nuclear localization of TFE3 to inhibit lysosomal biogenesis,[43] whereas mitochondrial translocation of TFEB also regulates complex I and inflammation.[44] Now our results suggest RAB32 expression, likely in response to TFE3-induction, provides a reciprocal mechanism to increase LRRK2 kinase activity in a circuit we term the "RAB32 rheostat" (**Supplementary Figure 8**). In myeloid-derived cells this mechanism helps regulate autophagosomal capacity for pathogen clearance by macrophages,[45] allergic response by mast cells,[46] and controls antigen presentation by dendritic cells.[34] However, to understand the roles of RAB32 and LRRK2 hyperactivity on immune surveillance, synaptic pruning and phagocytosis by microglia[47,48], and on dopaminergic neuronal survival in PD, demands further studies in model systems based on this insight.

From these data, we also postulate reduced/incomplete penetrance in individuals and families with *LRRK2* mutations [12,13] is a function of *RAB32* expression driven by intermittent peripheral immune activation throughout their lifespan. Such a hypothesis is consistent with PD as a multifactorial disease, manifest with age and inflammatory exposures, and may provide an elegant molecular explanation for the body-first hypothesis of PD.[49] It would also be consistent with the inverse association between the use of non-steroidal anti-inflammatory medications in *LRRK2*[50] and idiopathic PD[51]. Population differences in pathogen exposure may explain the disparity in disease penetrance in LRRK2 Gly2019Ser heterozygotes in Tunisia versus Norway, given that the cumulative incidence of idiopathic PD is almost identical.[13] The inter-individual variance in *RAB32* expression in human subjects has yet to be assessed but may be an important consideration for the success of clinical trials of Lrrk2 kinase inhibitors.[52] The GTEx Portal[53] shows many single nucleotide polymorphisms in the *RAB32* locus are correlated with its

expression in different tissues, including peripheral nerve and brain, and further studies of related genetic and biomarker variation in multi-incident *LRRK2* pedigrees may inform disease penetrance.

RAB32 biology provides an unequivocal physiologic and molecular conduit that unites research observations in PD including its clinical presentation, epidemiologic risk factors and prior Mendelian gene discoveries. This thesis can be viewed from an evolutionary genetic perspective, driven by the relationship between humans and pathogens. RAB32 expression, LRRK2 kinase activity, TFEB/TFE3 phosphorylation, and subsequent translocation to the nucleus or mitochondria appears to be intimately controlled from the lysosomal compartment to modulate peripheral and central immune responses[54], metabolism and dopaminergic cell survival. This nexus warrants future investment to develop therapeutic interventions in PD that offer more than symptomatic benefit.

Acknowledgements

This study was supported in part by research grants from the Michael J. Fox Foundation (MJFF-025964; awarded to MJF) and the Center for Translational Research in Neurodegenerative Disease (CTRND; awarded to JF and MJF). We thank the animal care staff at the McKnight Brain Institute and the Cancer and Genetics Research Complex, University of Florida, Gainesville, Florida, USA, the CTRND at the University of Florida for its technical support and access to shared equipment and Dr. Dario Alessi and the MRC PPU Reagents and Services at the University of Dundee for contributing Rab32 plasmids to this study. We also thank Dr. John Landers (UMass Chan Medical School, Worcester MA), Dr. Mark Cookson (NIA/NIH, Bethesda, MD) and the iPSC Neurodegenerative Disease Initiative (iNDI) for the iPSC cell lines, protocols and technical support.

Contributions

J.F.: conceptualization and project design, data curation, formal analysis, writing original draft, review and editing, and funding; I.B.D.: conceptualization and project design, data curation and formal analysis, writing original draft, review and editing; R.C.S.: conceptualization and project design, data curation and formal analysis, writing original draft; review and editing; S.W.: data curation, editing and reviewing; M.J.F.: resources and funding, conceptualization, writing, editing and reviewing.

Competing interests

The authors declare no competing interests.

REFEREENCES

1. Trinh, J. *et al.* A comparative study of Parkinson's disease and leucine-rich repeat kinase 2 p.G2019S parkinsonism. *Neurobiology of Aging* **35**, 1125–1131 (2014).
2. Mata, I. F. *et al.* Lrrk2 R1441G-related Parkinson's disease: Evidence of a common founding event in the seventh century in Northern Spain. *Neurogenetics* **10**, 347–353 (2009).
3. Farrer, M. J. *et al.* Lrrk2 G2385R is an ancestral risk factor for Parkinson's disease in Asia. *Parkinsonism and Related Disorders* **13**, 89–92 (2007).
4. Kachergus, J. *et al.* Identification of a novel LRRK2 mutation linked to autosomal dominant parkinsonism: evidence of a common founder across European populations. *American journal of human genetics* **76**, 672–680 (2005).
5. Guenther, D. T. *et al.* The Evolution of Genetic Variability at the LRRK2 Locus. *Genes (Basel)* **15**, 878 (2024).
6. Dzamko, N. L. LRRK2 and the Immune System. *Advances in neurobiology* **14**, 123–143 (2017).

7. Shutinoski, B. *et al. Lrrk2 Alleles Modulate Inflammation during Microbial Infection of Mice in a Sex-Dependent Manner*. *Sci. Transl. Med* vol. 11 9292 https://www.science.org (2019).

8. Alessi, D. R. & Sammler, E. LRRK2 kinase in Parkinson's disease. *Science* **360**, 36–37 (2018).

9. Kuhlmann, N. & Milnerwood, A. J. A Critical LRRK at the Synapse? The Neurobiological Function and Pathophysiological Dysfunction of LRRK2. *Frontiers in Molecular Neuroscience* **13**, 571518 (2020).

10. Zimprich, A. *et al.* Mutations in LRRK2 cause autosomal-dominant parkinsonism with pleomorphic pathology. *Neuron* **44**, 601–607 (2004).

11. Sekiya, H. *et al.* Widespread distribution of α-synuclein oligomers in LRRK2-related Parkinson's disease. *Acta Neuropathol* **149**, 42 (2025).

12. Healy, D. G. *et al.* Phenotype, genotype, and worldwide genetic penetrance of LRRK2-associated Parkinson's disease: a case-control study. *The Lancet Neurology* **7**, 583–590 (2008).

13. Hentati, F. *et al.* LRRK2 parkinsonism in Tunisia and Norway: A comparative analysis of disease penetrance. *Neurology* **83**, 568–569 (2014).

14. Marder, K. *et al.* Age-specific penetrance of LRRK2 G2019S in the Michael J. Fox Ashkenazi Jewish LRRK2 Consortium. *Neurology* **85**, 89–95 (2015).

15. Purlyte, E. *et al.* Rab29 activation of the Parkinson's disease-associated LRRK2 kinase. *The EMBO Journal* **37**, 1–18 (2018).

16. Gomez, R. C., Wawro, P., Lis, P., Alessi, D. R. & Pfeffer, S. R. Membrane association but not identity is required for LRRK2 activation and phosphorylation of Rab GTPases. *Journal of Cell Biology* **218**, 4157–4170 (2019).

17. Brighouse, A., Dacks, J. B. & Field, M. C. Rab protein evolution and the history of the eukaryotic endomembrane system. *Cell Mol Life Sci* **67**, 3449–3465 (2010).

18. McGrath, E., Waschbüsch, D., Baker, B. M. & Khan, A. R. LRRK2 binds to the Rab32 subfamily in a GTP-dependent manner via its armadillo domain. *Small GTPases* **12**, 133–146 (2021).

19. MacLeod, D. A. *et al.* RAB7L1 interacts with LRRK2 to modify intraneuronal protein sorting and Parkinson's disease risk. *Neuron* **77**, 425–39 (2013).

20. Beilina, A. *et al.* Unbiased screen for interactors of leucine-rich repeat kinase 2 supports a common pathway for sporadic and familial Parkinson disease. *Proc Natl Acad Sci U S A* **111**, 2626–2631 (2014).

21. Kalogeropulou, A. F. *et al.* Endogenous Rab29 does not impact basal or stimulated LRRK2 pathway activity. *Biochemical Journal* **477**, 4397–4423 (2020).

22. Gustavsson, E. K. *et al.* RAB32 Ser71Arg in autosomal dominant Parkinson's disease: linkage, association, and functional analyses. *The Lancet Neurology* **0**, (2024).

23. Hop, P. J. *et al.* Systematic rare variant analyses identify RAB32 as a susceptibility gene for familial Parkinson's disease. *Nature Genetics 2024 56:7* **56**, 1371–1376 (2024).

24. Radefeldt, M. *et al.* Genetic and Epidemiological Insights into RAB32-Linked Parkinson's Disease. *Mov Disord* **40**, 147–151 (2025).

25. Deng, I. B., Follett, J., Fox, J. D., Wall, S. & Farrer, M. J. Central biogenic amine deficiency with concomitant exploratory behavioral deficits in Dnajc12 knock-out mice. *NPJ Parkinsons Dis* **11**, 143 (2025).

26. Brownjohn, P. W. *et al.* Functional Studies of Missense TREM2 Mutations in Human Stem Cell-Derived Microglia. *Stem Cell Reports* **10**, 1294–1307 (2018).

27. Liang, Y. *et al.* Expression profiling of Rab GTPases reveals the involvement of Rab20 and Rab32 in acute brain inflammation in mice. *Neuroscience letters* **527**, 110–114 (2012).

28. Bu, M. *et al.* Inhibition of LRRK2 kinase activity rescues deficits in striatal dopamine physiology in VPS35 p.D620N knock-in mice. *npj Parkinson's Disease 2023 9:1* **9**, 1–12 (2023).

29. Zhu, H. *et al.* Rab29-dependent asymmetrical activation of leucine-rich repeat kinase 2. *Science* **382**, 1404–1411 (2023).

30. Karlsson, M. *et al.* A single–cell type transcriptomics map of human tissues. *Science Advances* **7**, eabh2169 (2021).

31. Program (GP2), T. G. P. G. & Leonard, H. L. Novel Parkinson's Disease Genetic Risk Factors Within and Across European Populations. 2025.03.14.24319455 Preprint at https://doi.org/10.1101/2025.03.14.24319455 (2025).

32. Bonet-Ponce, L. & Cookson, M. R. LRRK2 recruitment, activity, and function in organelles. *The FEBS Journal* (2021).

33. Festa, B. P. *et al.* Microglial-to-neuronal CCR5 signaling regulates autophagy in neurodegeneration. *Neuron* **111**, 2021-2037.e12 (2023).

34. Tandon, N. *et al.* The Rab32 small GTPase is required for efficient cross-priming of CD8+ T cells against cell-associated antigens by XCR1+ type 1 DCs in vivo. 2025.05.03.652057 Preprint at https://doi.org/10.1101/2025.05.03.652057 (2025).

35. Song, R. *et al.* The Rab32-LRMDA-Retriever Complex is a Key Regulator of Intestinal Immune Homeostasis. 2025.07.16.665158 Preprint at https://doi.org/10.1101/2025.07.16.665158 (2025).

36. Aksan, I. & Goding, C. R. Targeting the Microphthalmia Basic Helix-Loop-Helix–Leucine Zipper Transcription Factor to a Subset of E-Box Elements In Vitro and In Vivo. *Molecular and Cellular Biology* **18**, 6930–6938 (1998).

37. Sardiello, M. *et al.* A Gene Network Regulating Lysosomal Biogenesis and Function. *Science* **325**, 473–477 (2009).

38. Brunialti, E. *et al.* Design and validation of a reporter mouse to study the dynamic regulation of TFEB and TFE3 activity through in vivo imaging techniques. *Autophagy* **20**, 1879–1894 (2024).

39. Drizyte-Miller, K., Chen, J., Cao, H., Schott, M. B. & McNiven, M. A. The small GTPase Rab32 resides on lysosomes to regulate mTORC1 signaling. *Journal of Cell Science* **133**, (2020).

40. Li, X. *et al.* Emerging roles of TFE3 in metabolic regulation. *Cell Death Discov* **9**, 93 (2023).

41. Pastore, N. *et al.* TFE3 regulates whole-body energy metabolism in cooperation with TFEB. *EMBO Molecular Medicine* **9**, 605–621 (2017).

42. Martina, J. A., Diab, H. I., Brady, O. A. & Puertollano, R. TFEB and TFE3 are novel components of the integrated stress response. *The EMBO Journal* **35**, 479–495 (2016).

43. Yadavalli, N. & Ferguson, S. M. LRRK2 suppresses lysosome degradative activity in macrophages and microglia through MiT-TFE transcription factor inhibition. *Proceedings of the National Academy of Sciences of the United States of America* **120**, (2023).

44. Calabrese, C. *et al.* Mitochondrial translocation of TFEB regulates complex I and inflammation. *EMBO Rep* **25**, 704–724 (2024).

45. Zanocco-Marani, T. *et al.* Tfe3 expression is closely associated to macrophage terminal differentiation of human hematopoietic myeloid precursors. *Exp Cell Res* **312**, 4079–4089 (2006).

46. Yagil, Z. *et al.* Transcription factor E3, a major regulator of mast cell-mediated allergic response. *J Allergy Clin Immunol* **129**, 1357-1366.e5 (2012).

47. Volta, M. *et al.* Initial elevations in glutamate and dopamine neurotransmission decline with age, as does exploratory behavior, in LRRK2 G2019S knock-in mice. *eLife* **6**, (2017).

48. Zhang, Q. *et al.* Age-related LRRK2 G2019S Mutation Impacts Microglial Dopaminergic Fiber Refinement and Synaptic Pruning Involved in Abnormal Behaviors. *J Mol Neurosci* **72**, 527–543 (2022).

49. Borghammer, P. The brain-first vs. body-first model of Parkinson's disease with comparison to alternative models. *J Neural Transm (Vienna)* **130**, 737–753 (2023).

50. Luciano, M. S. *et al.* NON-STEROIDAL ANTI-INFLAMMATORY USE AND LRRK2 PARKINSON'S DISEASE PENETRANCE. *Mov Disord* **35**, 1755–1764 (2020).

51. Badawoud, A. M. *et al.* The relation between Parkinson's disease and non-steroidal anti-inflammatories; a systematic review and meta-analysis. *Front Pharmacol* **15**, 1434512 (2024).

52. Biogen bets $1B-plus on Denali's anti-LRRK2 Parkinson's program. https://www.fiercebiotech.com/biotech/biogen-bets-1b-denali-s-anti-lrrk2-parkinson-s-program.

53. Lonsdale, J. *et al.* The Genotype-Tissue Expression (GTEx) project. *Nat Genet* **45**, 580–585 (2013).

54. Wallings, R. L., Herrick, M. K. & Tansey, M. G. LRRK2 at the Interface Between Peripheral and Central Immune Function in Parkinson's. *Front Neurosci* **14**, 443 (2020).

55. Sha, Y., Rao, L., Settembre, C., Ballabio, A. & Eissa, N. T. STUB1 regulates TFEB-induced autophagy-lysosome pathway. *EMBO J* **36**, 2544–2552 (2017).

56. Martinez Fiesco, J. A. *et al.* 14-3-3 binding maintains the Parkinson's associated kinase LRRK2 in an inactive state. *Nat Commun* **16**, 7226 (2025).

57. Bentley-DeSousa, A., Roczniak-Ferguson, A. & Ferguson, S. M. A STING–CASM–GABARAP pathway activates LRRK2 at lysosomes. *Journal of Cell Biology* **224**, e202310150 (2025).

58. Medina, D. L. *et al.* Lysosomal calcium signalling regulates autophagy through calcineurin and TFEB. *Nat Cell Biol* **17**, 288–299 (2015).

59. Nakamura, S. *et al.* LC3 lipidation is essential for TFEB activation during the lysosomal damage response to kidney injury. *Nat Cell Biol* **22**, 1252–1263 (2020).

60. Zhao, J.-F. *et al.* Targeted dephosphorylation of TFEB promotes its nuclear translocation. *iScience* **27**, 110432 (2024).

61. Alto, N. M., Soderling, J. & Scott, J. D. Rab32 is an A-kinase anchoring protein and participates in mitochondrial dynamics. *Journal of Cell Biology* **158**, 659–668 (2002).

62. Bui, M. *et al.* Rab32 modulates apoptosis onset and mitochondria-associated membrane (MAM) properties. *J. Biol. Chem.* **285**, 31590–31602 (2010).

63. Chen, P. *et al.* Rab32 promotes glioblastoma migration and invasion via regulation of ERK/Drp1-mediated mitochondrial fission. *Cell Death Dis* **14**, 198 (2023).

64. Zhang, H.-L. *et al.* Rab32-based vesicles coordinate mitochondria and actin for spindle migration and organelle rearrangement in oocyte meiosis. *Journal of Advanced Research* (2025) doi:10.1016/j.jare.2025.05.001.

65. Lu, S.-L. *et al.* Evidence that mitochondria in macrophages are destroyed by microautophagy. *Nat Commun* **16**, 8123 (2025).

66. Johnson, K. M. *et al.* Rab32 regulates Golgi structure and cell migration through Protein Kinase A–mediated phosphorylation of Optineurin. *Proceedings of the National Academy of Sciences* **122**, e2502971122 (2025).

67. Schuster, E.-M. *et al.* TFEB induces mitochondrial itaconate synthesis to suppress bacterial growth in macrophages. *Nat Metab* **4**, 856–866 (2022).

68. Lian, H. *et al.* Parkinson's disease kinase LRRK2 coordinates a cell-intrinsic itaconate-dependent defence pathway against intracellular Salmonella. *Nature microbiology* **8**, 1880–1895 (2023).

69. Nezich, C. L., Wang, C., Fogel, A. I. & Youle, R. J. MiT/TFE transcription factors are activated during mitophagy downstream of Parkin and Atg5. *J Cell Biol* **210**, 435–450 (2015).

70. Cui, Y. *et al.* Formation of retromer transport carriers is disrupted by the Parkinson disease-linked Vps35 D620N variant. *Traffic* **22**, 123–136 (2021).

71. Vides, E. G. *et al.* A feed-forward pathway drives LRRK2 kinase membrane recruitment and activation. *eLife* **11**, (2022).

Figure 1: Expression of Rab32 and Rab38 are inversely associated with Rab29 and promote Rab10 phosphorylation.

A) Representative WB data of siRNA-mediated antibody validation in B16 cells for Rab32-sub family of GTPases, Lrrk2, Lamp1 and pRab10/Rab10. Data is representative of three independent experiments.

B) Quantification of protein lysates analyzed in (**A)** Data presented as mean ± S.E.M. Statistical analysis was determined through a One-way ANOVA with a Tukey multiple comparisons post-hoc test, where significant findings are reported relative to NTC. *: P-value ≤ 0.05; **: P-value ≤ 0.01; ***: P-value ≤ 0.001; ****: P-value ≤ 0.0001.

C) Relative gene expression ($2^{(-\Delta\Delta CT)}$) of Rab32-sub family of GTPases in B16 cells following siRNA-mediated knockdown. Data is pooled from three independent experiments where each dot on the graph represents an individual well that underwent the treatment paradigm. Data presented as mean ± S.E.M. Statistical analysis was analyzed using a repeated-measure one-way ANOVA with a Tukeys multiple comparisons post hoc test. *: P-value ≤ 0.05; **: P-value ≤ 0.01; ***: P-value ≤ 0.001; ****: P-value ≤ 0.0001.

Figure 2: Peripheral Administration of LPS Upregulates Expression of Rab32 and Increases Rab10 Phosphorylation in the Midbrain of WT Mice

A) Relative gene expression ($2^{(-\Delta\Delta CT)}$) of in the midbrain of WT mice assessed by qPCR at 6 and 24hrs post-injection with 1 mg/kg of LPS or saline control. Each dot on the graph represents an individual animal that underwent the treatment paradigm. Data presented as mean ± S.E.M.

B) Western blot analysis of RIPA-soluble midbrain lysates at 6 and 24hrs post-injection with 1 mg/kg of LPS or saline control. Approximately 10-20ug of protein was resolved for each sample, expect for the detection of pRab10, which required 40ug.

C) Quantification of western blots shown in **(B)** normalized to total Rab10 or Gapdh loading control. Each dot on the graph represents an individual animal that underwent the treatment paradigm. Data presented as mean ± S.E.M and analyzed by one-way ANOVA.

Figure 3: Sagittal Ideogram of Regional Gene Expression ($2^{(-\Delta\Delta CT)}$) of Rab32 in the Brain of Wild Type Mice with LPS

Relative gene expression ($2^{(-\Delta\Delta CT)}$) of *Rab32* from the prefrontal cortex (PFC), striatum (STR), hippocampus (HP), midbrain (MB), cerebellum (CB) and brain stem (BS) of WT mice were assessed by qPCR after 6 and 24hrs post-injection with 1 mg/kg of peripheral LPS or saline control. Brain mapping to a sagittal ideogram of the mouse brain was created by determining Log2 fold change (FC) of $2^{(-\Delta\Delta CT)}$ of each examined gene between saline control and either 6hrs or 24hrs cohorts. Heatmaps of Log2 FC were created and transposed onto a sagittal mouse brain ideogram of an H&E stain derived from the GENESTAT Project (https://gensat.org/) (see **Sup Figure 3** for original brain slice images used). Statistical analysis was determined through a two-way ANOVA with a Tukey multiple comparisons post-hoc test, where significant findings between saline control and 6hrs or 24hrs cohorts were reported by stars drawn on the brain region. *: P-value ≤ 0.05; **: P-value ≤ 0.01; ***: P-value ≤ 0.001; ****: P-value ≤ 0.0001. Comparative statistical analysis of gene expression with/without peripheral LPS treatment (6hr and 24hr), within all 6 brain regions, is provided by two-way ANOVA (**Supplemental Table 2)**. The

relative gene expression of each individual gene examined within each brain region by one-way ANOVA (**Supplementary Figure 4)**.

Figure 4: Membrane Localization of Rab32 is Necessary to Drive LRRK2 Activity

A) Representative WB data of HEK293 lysates transiently co-transfected with FLAG-LRRK2 and HA-Rab32 variants probed for FLAG (LRRK2), pS935, pS1292, pRab10, Rab10, HA(Rab32) and GAPDH.

B) Quantification of pS935/FLAG(LRRK2) in (**A)** Data presented as mean ± S.E.M. Statistical analysis was determined through a two-way ANOVA with a Tukey multiple comparisons post-hoc test, where significant findings are reported as *: P-value ≤ 0.05; **: P-value ≤ 0.01; ***: P-value ≤ 0.001; ****: P-value ≤ 0.0001.

C) Quantification of pS1292, pRab10 and HA data presented in (**A)** Data presented as mean ± S.E.M. Statistical analysis was determined through a two-way ANOVA with a Tukey multiple comparisons post-hoc test, where significant findings are reported as *: P-value ≤ 0.05; **: P-value ≤ 0.01; ***: P-value ≤ 0.001; ****: P-value ≤ 0.0001.

D) Representative WB data of Co-immunoprecipitated LRRK2-Rab32 complexes from HEK293 lysates transiently co-transfected with FLAG-LRRK2 and HA-Rab32 variants probed for FLAG (LRRK2), pS935, pS1292, pRab10, Rab10, HA(Rab32) and GAPDH.

E) Quantification of co-immunoprecipitated LRRK2 in HEK293 cells in **(E)** Data are normalized to total LRRK2 and presented as mean ± S.E.M

Figure 5: Peripheral Administration of LPS in WT Mice Upregulates Expression of Rab32 in Microglia but not DA Neurons in SN.

A) Representative confocal images of Iba1, Lamp1, Rab32, and their Imaris render, in the midbrain of mice injected with either LPS or saline. Sections are counterstained with DAPI.

B) Volumetric analysis of total Lamp1+ puncta. Statistical analysis was assessed by an unpaired *t*-test, $t_{26} = 0.14$, $p = 0.89$. Volumetric analysis of Lamp1+ puncta within Iba1+ microglia. Statistical analysis was assessed by an unpaired *t*-test, $t_{25} = 5.32$, $p<0.0001$. Volumetric analysis of total Rab32+ puncta. Statistical analysis was assessed by an unpaired *t*-test, $t_{26} = 2.22$, $p = 0.035$. Volumetric analysis of Rab32+ puncta within Iba1+ microglia. Statistical analysis was assessed by an unpaired *t*-test, $t_{26} = 3.85$, $p = 0.0007$. Raw volumetric analysis of microglial Rab32 localized to their lamp1+ lysosomes. Statistical analysis was assessed by an unpaired *t*-test, $t_{26} = 3.08$, $p = 0.0049$.

C) Representative confocal images of Th, Lamp1, Rab32, and their Imaris render, in the midbrain of mice injected with either LPS or saline. Sections are counterstained with DAPI.

D) Volumetric analysis of total Lamp1+ puncta. Statistical analysis was assessed by an unpaired *t*-test, t21 = 0.75, $p = 0.46$. Volumetric analysis of Lamp1+ puncta within DA+ neurons. Statistical analysis was assessed by an unpaired *t*-test, $t_{21} = 0.48$, $p = 0.64$. Volumetric analysis of total Rab32+ puncta. Statistical analysis was assessed by an unpaired *t*-test, $t_{21} = 2.29$, p = 0. 034.Volumetric analysis of Rab32+ puncta within in DA+ neurons. Statistical analysis was assessed by an unpaired *t*-test, $t_{21} = 0.39$, p = 0.70). Raw volumetric analysis of DA neuron restricted Rab32 localized to their lamp1+ lysosomes Unpaired *t*-test, $t_{21} = 1.90$, $p = 0.07$).

*p□<□0.05, **p□<□0.01, ***p□<□0.001, ****p□<□0.0001. Error bars are□±□SEM. n refers to the number of mice and in parentheses the number of sections [3□M old mice, Sal n□=□7 (14); LPS n□=□7 (14)].

Supp Figure 1: Validation of Antibodies Against Rab32, Rab38 and Ra29 by Immunocytochemistry in B16 Cells.

A) Representative confocal microscopy images of endogenous Rab32, Rab38 or Rab29 with and without targeting siRNAs. Cells are counterstained with DAPI.

B) Quantification of fluorescence intensity for microscopy images presented in A.

Supp Figure 2: Rab32 is necessary to support Rab10 phosphorylation and Lamp1 levels

A) Representative WB data of siRNA-mediated knockdown in B16 cells for Rab32-sub family of GTPases, Lrrk2, Lamp1 and pRab10/Rab10. Data is representative of three independent experiments.

B) Quantification of protein lysates analyzed in (**A)** Data presented as mean ± S.E.M. Statistical analysis was determined through a Two-way ANOVA with a Tukey multiple comparisons post-hoc test, where significant findings are reported relative to NTC. *: P-value ≤ 0.05; **: P-value ≤ 0.01; ***: P-value ≤ 0.001; ****: P-value ≤ 0.0001.

Supp Figure 3: Establishing a working inflammatory paradigm in WT mice

A) Relative gene expression ($2^{(-\Delta\Delta CT)}$) of immunoresponsive genes from WT mice were assessed by qPCR after 6 and 24hrs post-injection with 1 or 5mg/kg of peripheral LPS or

saline control. Data presented as mean ± S.E.M with eat dot representing an individual animal that underwent the treatment paradigm.

B) Western blot data of RIPA-soluble midbrain lysates from three-month old WT mice that received either saline control, 1mg/kg or 5mg/kg LPS.

C) Quantification of WB data presented in **A**. Each dot on the graph represents an individual animal that underwent the treatment paradigm. Data presented as mean ± S.E.M and analyzed by one-way ANOVA.

Supp Figure 4: Sagittal Ideogram of Regional Gene Expression ($2^{(-\Delta\Delta CT)}$) of Immunoresponsive and Rab GTPase Genes in the Brain of Wild Type mice with LPS

A) H&E stain used for **Figure 2** gene expression brain mapping. Derived from the GENESTAT Project at The Rockefeller University.

B) Sectional mapping used as example for **Figure 2**. Derived from the GENESTAT Project at The Rockefeller University.

C) Black and white image of H&E stain with relevant sections drawn out for **Figure 2**. Derived from the GENESTAT Project at The Rockefeller University.

D) Relative gene expression ($2^{(-\Delta\Delta CT)}$) of immunoresponsive genes from the prefrontal cortex (PFC), striatum (STR), hippocampus (HP), midbrain (MB), cerebellum (CB) and brain stem (BS) of WT mice were assessed by qPCR after 6 and 24hrs post-injection with 1 mg/kg of peripheral LPS or saline control. Brain mapping to a sagittal ideogram of the mouse brain was created by determining Log2 fold change (FC) of $2^{(-\Delta\Delta CT)}$ of each examined gene between saline control and either 6hrs or 24hrs cohorts. Heatmaps of Log2 FC were created and transposed onto a sagittal mouse brain ideogram of an H&E

stain (black and white colored) derived from the GENESTAT Project at The Rockefeller University (see **Sup Figure 2** for original brain slice images used). Statistical analysis was determined through a two-way ANOVA with a Tukey multiple comparisons post-hoc test, where significant findings between saline control and 6hrs or 24hrs cohorts were reported by stars drawn on the brain region. *: P-value ≤ 0.05; **: P-value ≤ 0.01; ***: P-value ≤ 0.001; ****: P-value ≤ 0.0001. Comparative statistical analysis of gene expression with/without peripheral LPS treatment (6hr and 24hr), within all 6 brain regions, is provided by two-way ANOVA (**Supplemental Table 2)**. The relative gene expression of each individual gene examined within each brain region by one-way ANOVA (**Supplementary Figure 4)**.

E) Relative gene expression ($2^{(-\Delta\Delta CT)}$) of Rab GTPase genes from the prefrontal cortex (PFC), striatum (STR), hippocampus (HP), midbrain (MB), cerebellum (CB) and brain stem (BS) of WT mice were assessed by qPCR after 6 and 24hrs post-injection with 1 mg/kg of peripheral LPS or saline control. Brain mapping to a sagittal ideogram of the mouse brain was created by determining Log2 fold change (FC) of $2^{(-\Delta\Delta CT)}$ of each examined gene between saline control and either 6hrs or 24hrs cohorts. Heatmaps of Log2 FC were created and transposed onto a sagittal mouse brain ideogram derived from the GENESTAT Project at Rockefeller University (see **Sup Figure 3** for original brain slice images used). Statistical analysis was determined through a two-way ANOVA with a Tukey multiple comparisons post-hoc test, where significant findings between saline control and 6hrs or 24hrs cohorts were reported by stars drawn on the brain region. *: P-value ≤ 0.05; **: P-value ≤ 0.01; ***: P-value ≤ 0.001; ****: P-value ≤ 0.0001. Comparative statistical analysis of gene expression with/without peripheral LPS

treatment (6hr and 24hr), within all 6 brain regions, is provided by two-way ANOVA (**Supplemental Table 2)**. The relative gene expression of each individual gene examined within each brain region by one-way ANOVA (**Supplementary Figure 3)**.

Supp Figure 5: One-Way ANOVA Bar Graphs of Gene Expression Examined Within Each Section of the Mouse Brain

A) Relative gene expression ($2^{(-\Delta\Delta CT)}$) of immunoresponsive genes from the prefrontal cortex (PFC), striatum (STR), hippocampus (HP), midbrain (MB), cerebellum (CB) and brain stem (BS) of WT mice were assessed by qPCR after 6 and 24hrs post-injection with 1 mg/kg of peripheral LPS or saline control. Data presented as mean ± S.E.M and analyzed by one-way ANOVA (parametric: Brown-Forsythe and Welch ANOVA tests with Dunnett T3 multiple comparisons post-hoc test; non-parametric: Kruskal-Wallis test with a Dunn's multiple comparison post-hoc test).

B) Relative gene expression ($2^{(-\Delta\Delta CT)}$) of Rab GTPase genes from the prefrontal cortex (PFC), striatum (STR), hippocampus (HP), midbrain (MB), cerebellum (CB) and brain stem (BS) of WT mice were assessed by qPCR after 6 and 24hrs post-injection with 1 mg/kg of peripheral LPS or saline control. Data presented as mean ± S.E.M and analyzed by one-way ANOVA (parametric: Brown-Forsythe and Welch ANOVA tests with Dunnett T3 multiple comparisons post-hoc test; non-parametric: Kruskal-Wallis test with a Dunn's multiple comparison post-hoc test).

Supp Figure 6: LPS induces Rab32 expression in iPSC-derived IBA1+ microglia

A) Representative confocal microscopy images of endogenous Rab32 and IBA1 in IPSC-derived microglia treated with 100ng/mL LPS or saline control. Cells are counterstained with DAPI.

B) Quantification of fluorescence intensity for microscopy images presented in A. Data is representative of > 100 cells quantified across 3-independent experiments. Error bars mean ± SEM. Statistical analysis was determined through a two-way Mann-Whitney T-test, **P < 0.01.

Supp Figure 7: Comparative analysis of RAB32, 38 and 29 promoter sequences

Promoter sequences including 250bp 5' of the start of transcription (TSS) to the start of translation (annotated in grey) are illustrated for each gene. A search for CLEAR sequence motifs revealed no perfect match to the GTCACGTGAC consensus. However, CLEAR-2 (red) and CLEAR-3 (orange) mismatches were identified, with 80% or 70% identity, respectively. Notably, Rab32, RAB32 and RAB38 have 5' CLEAR-2 sites that match criteria for E-box sequences (CANNTG) known to bind transcription factor 3 (TFE3).[36] However, the greatest affinity for transcription factor binding and gene expression is mediated by "tandem" CLEAR motifs within −195 to −118 base pairs 5' of the TSS[38] and only the promoters of Rab32/RAB32 approximate this configuration.

Genomic sequences and annotations were obtained from the Ensembl database for murine C57BL/6J [GRCm39] Rab32 (Genomic ENSMUSG00000019832; transcript ENSMUST00000019974.5; Rab32-201), Rab38 (Genomic ENSMUSG00000030559; transcript ENSMUST00000107256; Rab38-201) and Rab29 (Genomic ENSMUSG00000026433; transcript ENSMUST00000027693; Rab29-201) and human [GRCh38.p14] RAB32 (Genomic ENSG00000118508; transcript ENST00000367495; RAB32-201), RAB38 (Genomic ENSG00000123892; transcript ENST00000243662; RAB38-201) and RAB29 (Genomic

ENSG00000117280; transcript ENST00000367139; RAB29-201) loci (reference sequence identifiers).

Supp Figure 8: Graphical figure and abstract

Ideogram of RAB32 in myeloid cells, its complex relationship with mTOR on lysosomes, MiT transcription factors in lysosomal biogenesis and mitophagy, focused on the role of Mendelian genes implicated in Parkinson's disease. In a replete state RAB32, in a GTP/GDP independent manner, is recruited by heterodimeric Rag GTPase to lysosomes. This induces mTORC1 kinase activity to phosphorylate MiT transcription factors, S321 TFE3 and S211 TFEB[39] that enables 14-3-3 binding and cytoplasmic sequestration and/or proteosomal degradation through interaction with STUB1.[55] LRRK2 kept dormant in cytoplasm as part of a 14-3-3 complex[56] is recruited to lysosomes in response to stress, inflammation or damage to lysosomal membranes.[57] The abundance of lysosomal LRRK2 and its kinase activity negatively regulate the nuclear localization of MiT transcription factors.[43] Conversely, lysosomal calcium signaling regulates autophagy through TFEB dephosphorylation by calcineurin.[58,59] PP2A activation in response to oxidative stress may also trigger TFEB/3 dephosphorylation, inducing its nuclear translocation and subsequent transcriptional activity.[42,60] Furthermore, RAB32 determines the targeting of PKA to mitochondria, increasing the phosphorylation of Drp1, regulating fission and mitophagy[61–65]. Concomitantly, Rab32 regulates Golgi structure and cell migration through PKA-mediated phosphorylation of OPTN.[66] In macrophages, LPS and IFNγ signaling activates TFEB, the mitochondrial TCA-cycle, itaconate synthesis[67] and delivery to nascent autophagosomes, tethered by RAB32 and LRRK2.[68] Enhanced by mTOR inhibition, TFEB translocation to mitochondria then regulates complex 1 to down-modulate inflammation and the expression of pro-inflammatory cytokines.[44] MiT transcription factors are also activated during mitophagy downstream of PINK1 and Parkin.[69] Lastly, VPS35 is illustrated to highlight retromer's role in cation-independent receptor recycling. This is a prerequisite to enable the traffic of newly synthesized hydrolases from the trans-Golgi via maturing endosome to endolysosome and lysosome compartments.[70] RAB29 activates LRRK2 on Golgi and endosomal

membranes[15,71], although its expression is not essential on lysosomes[21] and is tied to the expression of its homologue, RAB32, by MiT transcription.

FIGURE 1

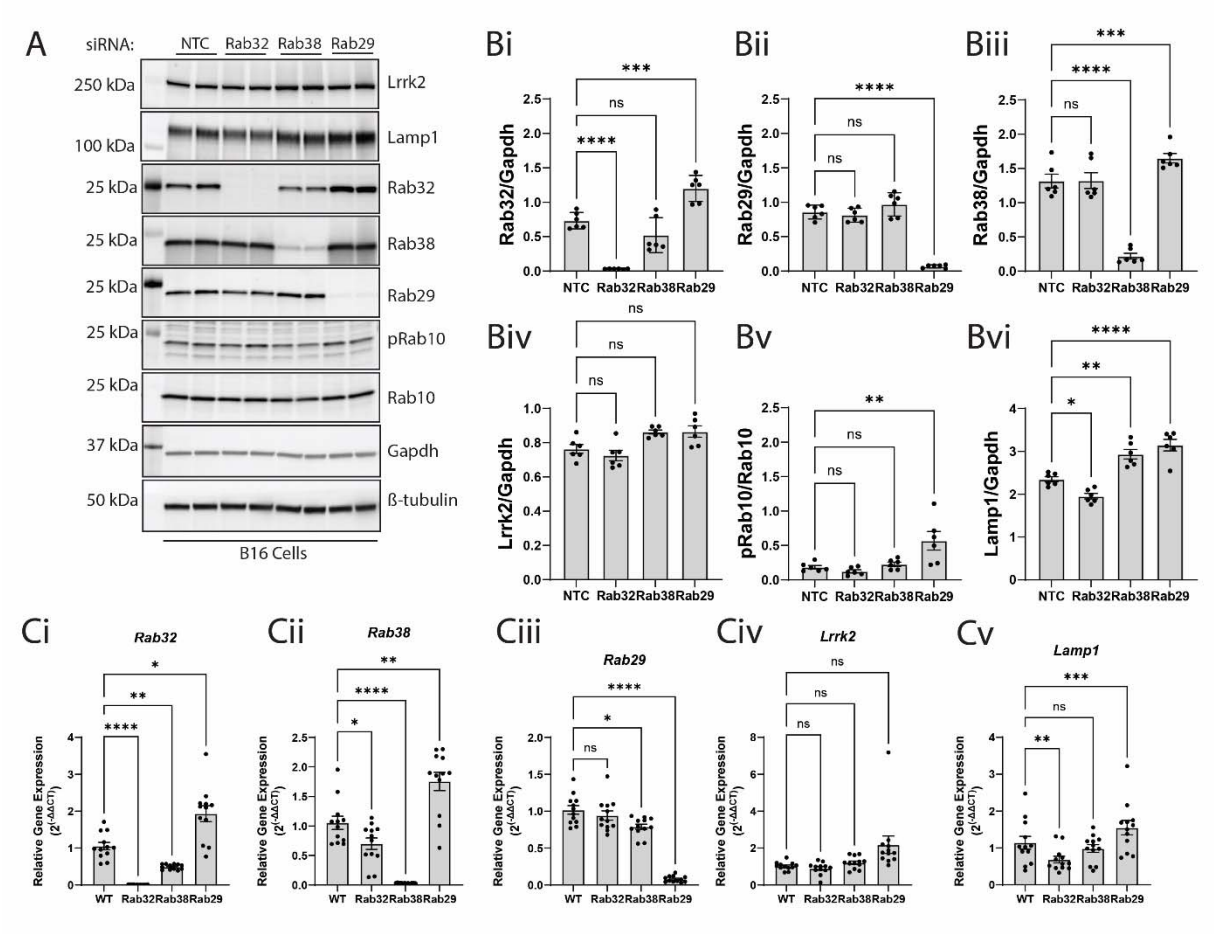
A
siRNA:
NTC
Rab32
Rab38
Rab29
250 kDa
Lrrk2
100 kDa
Lamp1
25 kDa
Rab32
25 kDa
Rab38
25 kDa
Rab29
25 kDa
pRab10
25 kDa
Rab10
37 kDa
Gapdh
50 kDa
ß-tubulin
B16 Cells
Bi
Rab32/Gapdh
Bii
Rab29/Gapdh
Biii
Rab38/Gapdh
Biv
Lrrk2/Gapdh
Bv
pRab10/Rab10
Bvi
Lamp1/Gapdh
NTC
Rab32
Rab38
Rab29
ns
Ci
Rab32
Cii
Rab38
Ciii
Rab29
Civ
Lrrk2
Cv
Lamp1
Relative Gene Expression
WT

FIGURE 2

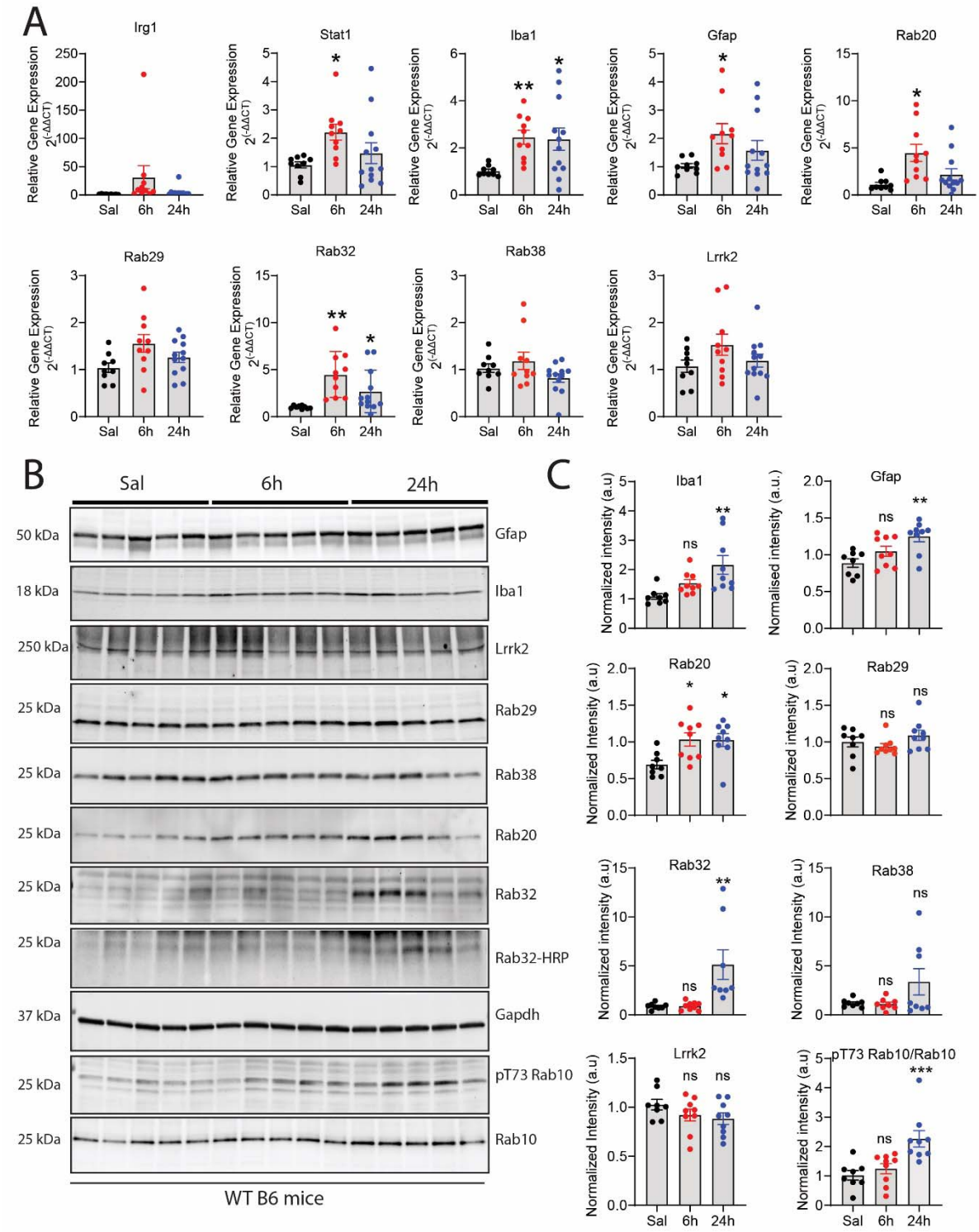
A
Irg1
Stat1
Iba1
Gfap
Rab20
Rab29
Rab32
Rab38
Lrrk2
Relative Gene Expression
2(-ΔΔCT)
Sal
6h
24h
B
Sal
6h
24h
50 kDa
Gfap
18 kDa
Iba1
250 kDa
Lrrk2
25 kDa
Rab29
25 kDa
Rab38
25 kDa
Rab20
25 kDa
Rab32
25 kDa
Rab32-HRP
37 kDa
Gapdh
25 kDa
pT73 Rab10
25 kDa
Rab10
WT B6 mice
C
Iba1
Gfap
Rab20
Rab29
Rab32
Rab38
Lrrk2
pT73 Rab10/Rab10
Normalized intensity (a.u)
Normalised intensity (a.u.)
Normalized Intensity (a.u)
ns

FIGURE 3

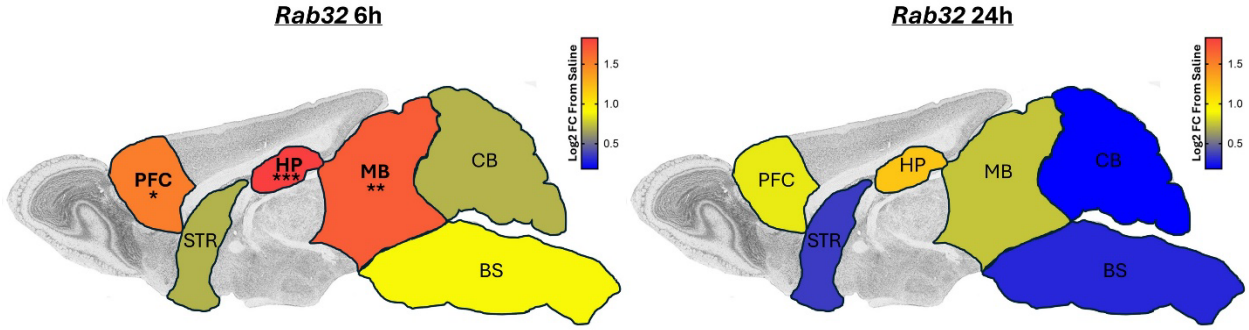
Rab32 6h
Log2 FC From Saline
1.5
1.0
0.5
PFC
*
HP
***
MB
**
CB
STR
BS
Rab32 24h
Log2 FC From Saline
1.5
1.0
0.5
PFC
HP
MB
CB
STR
BS

FIGURE 4

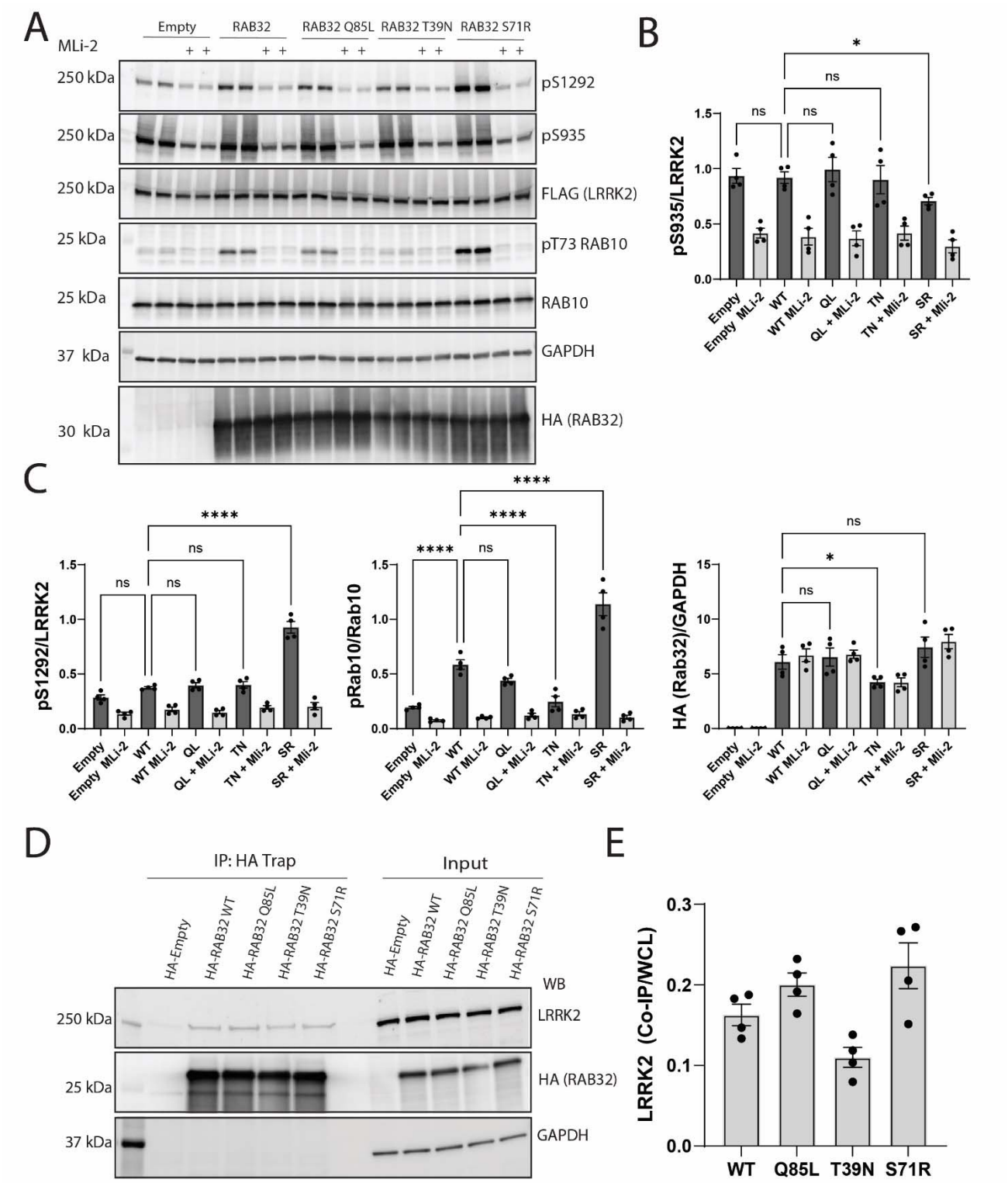
A
Empty
RAB32
RAB32 Q85L
RAB32 T39N
RAB32 S71R
MLi-2
250 kDa
pS1292
250 kDa
pS935
250 kDa
FLAG (LRRK2)
25 kDa
pT73 RAB10
25 kDa
RAB10
37 kDa
GAPDH
30 kDa
HA (RAB32)
B
pS935/LRRK2
C
pS1292/LRRK2
pRab10/Rab10
HA (Rab32)/GAPDH
Empty
Empty MLi-2
WT
WT MLi-2
QL
QL + MLi-2
TN
TN + Mli-2
SR
SR + Mli-2
D
IP: HA Trap
Input
HA-Empty
HA-RAB32 WT
HA-RAB32 Q85L
HA-RAB32 T39N
HA-RAB32 S71R
WB
250 kDa
LRRK2
25 kDa
HA (RAB32)
37 kDa
GAPDH
E
LRRK2 (Co-IP/WCL)
WT
Q85L
T39N
S71R

FIGURE 5

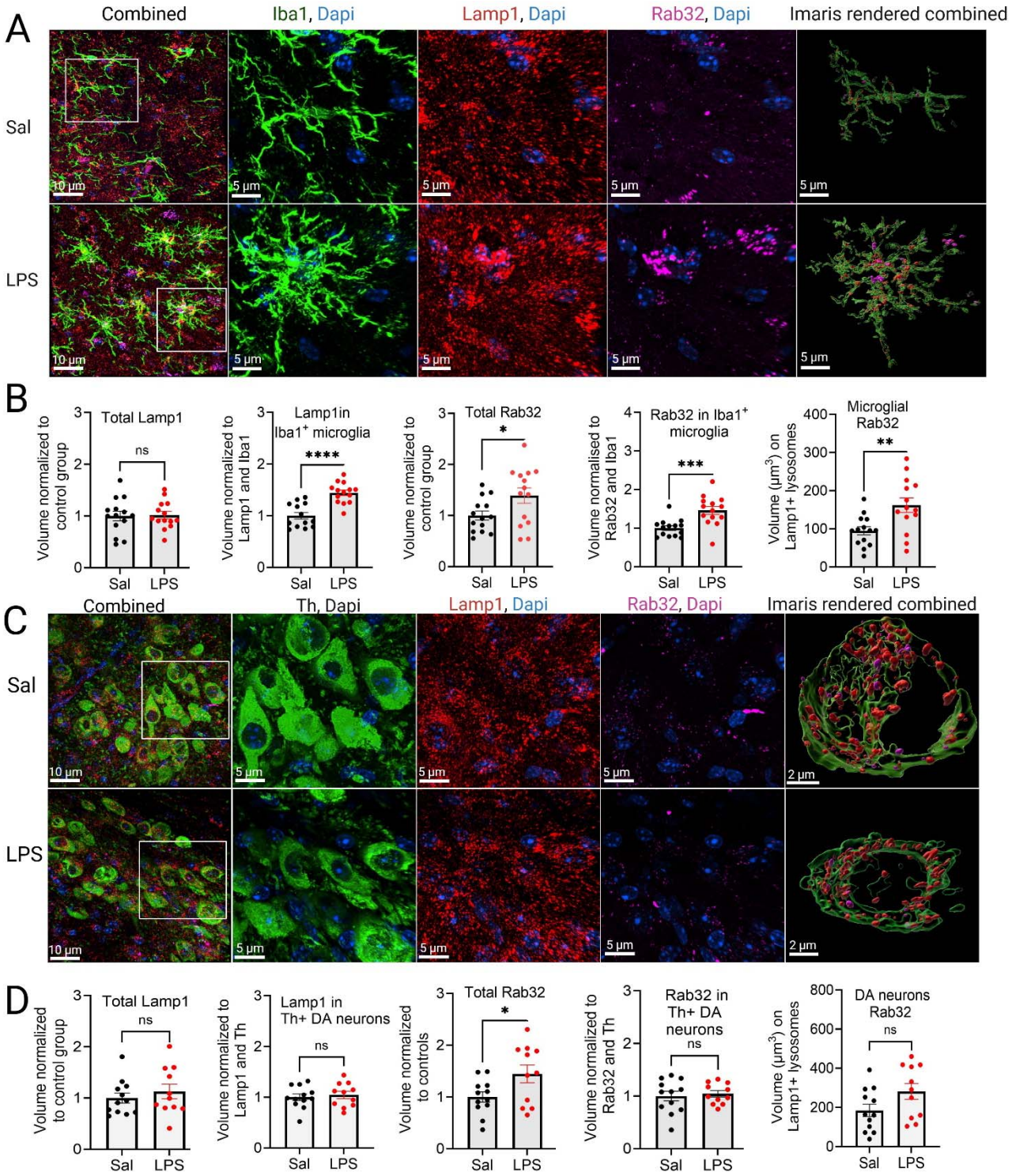
A
Combined
Iba1, Dapi
Lamp1, Dapi
Rab32, Dapi
Imaris rendered combined
Sal
LPS
10 µm
5 µm
B
Total Lamp1
ns
Lamp1in Iba1+ microglia
****
Total Rab32
*
Rab32 in Iba1+ microglia
***
Microglial Rab32
**
Volume normalized to control group
Volume normalized to Lamp1 and Iba1
Volume normalised to Rab32 and Iba1
Volume (µm3) on Lamp1+ lysosomes
Sal
LPS
C
Combined
Th, Dapi
Lamp1, Dapi
Rab32, Dapi
Imaris rendered combined
Sal
LPS
10 µm
5 µm
2 µm
D
Total Lamp1
ns
Lamp1 in Th+ DA neurons
ns
Total Rab32
*
Rab32 in Th+ DA neurons
ns
DA neurons Rab32
ns
Volume normalized to control group
Volume normalized to Lamp1 and Th
Volume normalized to controls
Volume normalized to Rab32 and Th
Volume (µm3) on Lamp1+ lysosomes
Sal
LPS